ACADEMIC PRESS

Available online at www.sciencedirect.com

SCIENCE DIRECT®

Journal of Computational Physics 186 (2003) 198–211

JOURNAL OF COMPUTATIONAL PHYSICS

www.elsevier.com/locate/jcp

Shape identification for natural convection problems using the adjoint variable method

H.M. Park *, H.J. Shin

Department of Chemical Engineering, Sogang University, Seoul, Republic of Korea

Received 27 November 2001; received in revised form 7 October 2002; accepted 11 January 2003

Abstract

An inverse geometry problem is investigated to identify the boundary shape of a domain from temperature measurements on the other boundary, where the temperature field is dominated by natural convection. The potential applications of the present investigation are the determination of a phase change isotherm in the Bridgman crystal growth or the thermal tomography which detects flaws in materials nondestructively. The inverse problem is posed as a minimization problem of the performance function, which is the sum of square residuals between calculated and observed temperature, by means of a conjugate gradient method employing the adjoint variable method. The present method is found to identify the domains reasonably accurately even with noisy temperature measurements.

Keywords: Shape identification; Natural convection; Adjoint variable method

1. Introduction

Domain identification problems arise in various branches of science and engineering. These are a class of inverse problems [1] and may be solved by various optimization techniques for partial differential equations. One interesting example is the thermal tomography [2]. The thermal tomography involves characterizing structural flaws caused by corrosion or cracks, which may not be detectable visually. By measuring temperature at certain locations on the boundary for a given heat flux, one can identify location of the system boundary, and thus may detect and characterize these structural flaws nondestructively. Another example is the identification of a phase change isotherm in the Bridgman crystal growth of semiconductor materials [3]. Since the phase change occurs at a constant temperature, the identification of an isotherm corresponding to the melting temperature is tantamount to the determination of the phase boundary. Since the curvature of the interface between the crystal and melt, together with the melt convection, causes radial segregation of dopants in the crystal, the identification of phase boundary is very important for the quality

* Corresponding author. Tel./fax: +82-2-705-8482.
E-mail address: hmpark@ccs.sogang.ac.kr (H.M. Park).

0021-9991/03/$ - see front matter
doi:10.1016/S0021-9991(03)00046-9

control of the Bridgman process. At last, we may mention the importance of the identification of location of the phase boundary in the direct solidification processes for cast turbine blades [4], where the velocity of freezing front is the main process variable that controls the final solidification microstructures. These shape identification problems are different from the optimal shape design problems which are motivated by numerous applications to structural, airplane and ship design [5–8].

In the present investigation, we consider some shape identification problems of natural convection system, where the location of the system boundary is determined from temperature measurements on the other boundary. After mapping the irregular domains into a reference one using a set of parameters, the inverse problem is formulated as a parameter optimization problem of the output least-squares criterion, which is solved by a conjugate gradient method. The governing equations are discretized by a finite volume method. Although more recent techniques such as the arbitrary mesh method with fully implicit solvers might have been employed, the finite volume method is still one of the most preferred techniques for solving the Navier–Stokes equations. The specific system under consideration is the following two-dimensional domain Ω with boundaries $\partial\Omega_i$ filled with a Boussinesq fluid (Fig. 1(a)). Natural convection is induced by the temperature gradient in the system. Governing equations in dimensionless variables may be written as:

$$\nabla \cdot \mathbf{v} = 0. \tag{1}$$

$$\frac{\partial \mathbf{v}}{\partial t} + \mathbf{v} \cdot \nabla \mathbf{v} = -\nabla P + P_r \nabla^2 \mathbf{v} + R P_r T \mathbf{j}, \tag{2}$$

$$\frac{\partial T}{\partial t} + \mathbf{v} \cdot \nabla T = \nabla^2 T. \tag{3}$$

Using superscript asterisk to denote dimensional quantities, the dimensionless variables are defined as follows

$$x = \frac{x^*}{d}, \quad y = \frac{y^*}{d}, \quad t = \frac{\kappa t^*}{d^2}, \quad \mathbf{v} = \frac{d\mathbf{v}^*}{\kappa}, \quad T = \frac{T^* - T^*_{\text{cold}}}{T^*_{\text{hot}} - T^*_{\text{cold}}}, \quad P' = \frac{d^2 P^*}{\rho \kappa^2}, \tag{4}$$

where T^* is the temperature, t^* is time, $\mathbf{v}^*$ is the velocity field, P^* is the pressure field, κ is the thermal diffusivity, ρ is the density, d is the characteristic length of the domain. In consistent with the Boussinesq approximation, we regard the physical properties of the fluid constant except the density in the body force term, which is represented as a function of temperature. The dimensionless group R is the Rayleigh number and P_r is the Prandtl number defined as follows:

$$R = \alpha g \frac{(T^*_{\text{hot}} - T^*_{\text{cold}}) d^3}{\kappa \nu}, \tag{5}$$

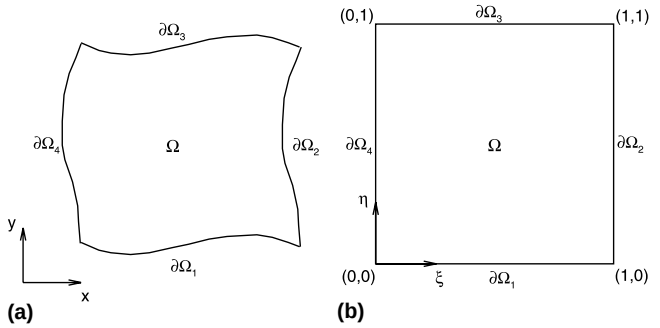

Fig. 1. (a) A general two-dimensional domain in the physical space. (b) Transformed domain in the computational space.

$$P_r = \frac{v}{\kappa}, \tag{6}$$

where α is the thermal expansion coefficient, g is the gravitational constant and v is the kinematic viscosity. The inverse problem under consideration is the identification of shapes of some boundaries $\partial\Omega_i$ from steady-state temperature measurements on the other boundaries. Although the present inverse problems are steady problems we keep time-derivative terms in Eqs. (2) and (3), since it is easier to solve the unsteady equation to yield the steady state solution than to solve the steady equations themselves for the Navier–Stokes problems. Recently a few shape identification problems for the heat conduction system and semiconductor devices have been published [9–12], but the shape identification problems for natural convection system have not been addressed frequently. Although Yang and Zabaras [13] and Park and Chung [14] consider inverse natural convection problems, these are inverse analyses on fixed domains.

2. System

We solve this shape identification problem after transforming the irregular system domains in the physical space (x, y) to a fixed square computational domain (ξ, η) as shown in Fig. 1(b). Then the governing equations using the dimensionless variables may be written in the computational domain as:

$$\frac{\partial V^i}{\partial \xi^i} = 0, \tag{7}$$

$$\sqrt{g}\frac{\partial \mathbf{v}}{\partial t} + \frac{\partial}{\partial \xi^i}(V^i \mathbf{v}) = \frac{\partial}{\partial \xi^i}\left[Prg^{ij}\sqrt{g}\frac{\partial \mathbf{v}}{\partial \xi^j}\right] - \frac{\partial}{\partial \xi^i}(\sqrt{g}\mathbf{g}^i P) + RPr\sqrt{g}T\mathbf{j}, \tag{8}$$

$$\sqrt{g}\frac{\partial T}{\partial t} + \frac{\partial}{\partial \xi^i}(V^i T) = \frac{\partial}{\partial \xi^i}\left[g^{ij}\sqrt{g}\frac{\partial T}{\partial \xi^j}\right], \tag{9}$$

where

$$\sqrt{g} = \frac{\partial x}{\partial \xi}\frac{\partial y}{\partial \eta} - \frac{\partial y}{\partial \xi}\frac{\partial x}{\partial \eta}, \tag{10}$$

$$\mathbf{g}^1 = \frac{1}{\sqrt{g}}\left(\mathbf{i}\frac{\partial y}{\partial \eta} - \mathbf{j}\frac{\partial x}{\partial \eta}\right), \tag{11}$$

$$\mathbf{g}^2 = \frac{1}{\sqrt{g}}\left(-\mathbf{i}\frac{\partial y}{\partial \xi} + \mathbf{j}\frac{\partial x}{\partial \xi}\right), \tag{12}$$

$$g^{ij} = \mathbf{g}^i \cdot \mathbf{g}^j, \tag{13}$$

$$V^i = \sqrt{g}\mathbf{g}^i \cdot \mathbf{v}. \tag{14}$$

The summation is over $i = 1, 2$ and, $\xi^1 = \xi$, $\xi^2 = \eta$. The above set of equations, with relevant boundary conditions, is solved by the finite volume method based on the SIMPLE algorithm [15]. Collocated arrangement of variables is adopted, where all the variables are stored at the same set of grid points and the same control volumes are used for all variables. Artificial pressure oscillation is prevented by employing the

Rhie–Chow interpolation scheme [16]. For simplicity, we adopt the following set of elliptic equations [17] for domain transformation and grid generation. But other grid generation techniques may be employed without further complications.

$$(\sqrt{g})^2 g^{11}\frac{\partial^2 x}{\partial \xi^2} + 2(\sqrt{g})^2 g^{12}\frac{\partial^2 x}{\partial \xi \partial \eta} + (\sqrt{g})^2 g^{22}\frac{\partial^2 x}{\partial \eta^2} = 0. \tag{15}$$

$$(\sqrt{g})^2 g^{11}\frac{\partial^2 y}{\partial \xi^2} + 2(\sqrt{g})^2 g^{12}\frac{\partial^2 y}{\partial \xi \partial \eta} + (\sqrt{g})^2 g^{22}\frac{\partial^2 y}{\partial \eta^2} = 0. \tag{16}$$

The shape identification problems investigated in the present paper are as follows. The shape and location of the boundaries $\partial\Omega_2$, $\partial\Omega_3$ and $\partial\Omega_4$ are fixed and known. We want to identify the location and shape of the boundary $\partial\Omega_1$ from temperature measurements on $\partial\Omega_3$. The temperatures on the boundaries $\partial\Omega_1$, $\partial\Omega_2$, and $\partial\Omega_4$ are given, and an adiabatic condition is imposed on the boundary $\partial\Omega_3$. The three domains shown in Fig. 2 are investigated in this work. The boundary conditions for Eqs. (7)–(9), (15), and (16) are:

- on $\partial\Omega_1$; $\mathbf{v} = 0$, $T = 1.0$, $x = 10\xi$, $y = F(x)$; (17)
- on $\partial\Omega_2$; $\mathbf{v} = 0$, $T = 0.0$, $x = 10.0$, $y = 1.5\eta$; (18)
- on $\partial\Omega_3$; $\mathbf{v} = 0$, $\dfrac{\partial T}{\partial y} = 0.0$, $x = 10\xi$, $y = 1.5$; (19)
- on $\partial\Omega_4$; $\mathbf{v} = 0$, $T = 0.0$, $x = 0.0$, $y = 1.5\eta$. (20)

The function $F(x)$ in Eq. (17) is the unknown to be determined. In these figures (Figs. 2(a)–(c)), the relevant boundary conditions and measurement points are also indicated. Figs. 3(a)–(c) show the typical velocity and temperature fields for these domains. The isotherms are indicated with dashed lines.

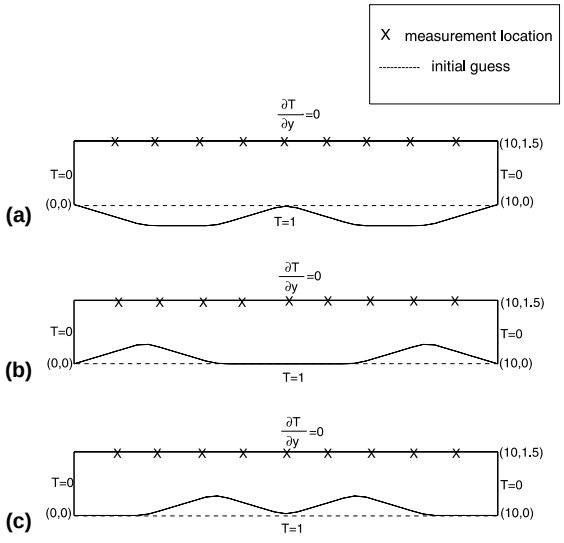

Fig. 2. (a)–(c) The domains and boundary conditions for the shape identification problems.

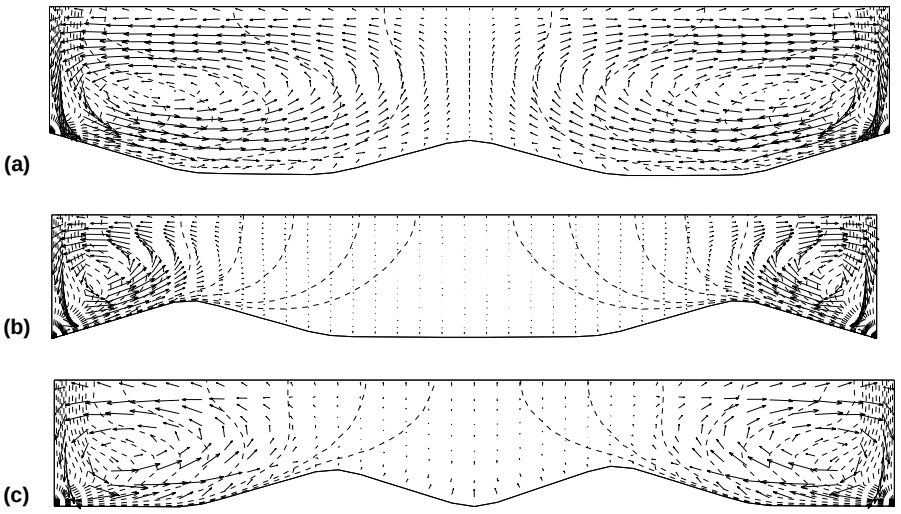

Fig. 3. (a)–(c) Typical velocity and temperature fields for the domains of Figs. 2(a)–(c).

3. Solution method for the identification problems

The inverse problem of identifying the shape of the domain is posed as a minimization problem of the following least-squares criterion.

$$J = \frac{1}{2}\sum_{m=1}^{\mathrm{MO}} (T(x_m, y_m) - T^*(x_m, y_m))^2, \tag{21}$$

where MO is the number of measurement points, (x_m, y_m) is the mth measurement location, $T^*(x_m, y_m)$ is the measured steady temperature and $T(x_m, y_m)$ is the computed steady temperature using the model. We try to find the shape of the domain defined by the geometric variable $F(x)$ such that the objective function J given in Eq. (21) is minimized. The minimization of the objective function is done using the conjugate gradient method [18,19]. The most crucial step in this method is the determination of the gradient function $\nabla J(F)$, which provides a measure of sensitivity of the objective function to the current geometric variable, F, available. In the present investigation, we determine ∇J by using the adjoint variable method. The gradient of the objective function ∇J is defined by

$$\delta J(F) \equiv J(F + \delta F) - J(F) = \langle \nabla J, \delta F \rangle, \tag{22}$$

where the bracket $\langle , \rangle$ denotes the inner product. Depending on the dimensionality of the geometric function F, we interpret the inner product operation differently. If F is infinite dimensional, i.e., $F = F(\xi)$, then ∇J is also infinite dimensional, and

$$\langle \nabla J, \delta F \rangle = \int_{\xi=0}^{1} \nabla J(\xi)\delta F(\xi)\,\mathrm{d}\xi. \tag{23}$$

On the other hand, when the geometric function $F(\xi)$ is discretized as

$$F(\xi) = \sum_{m=1}^{M} F_m \psi_m(\xi), \tag{24}$$

where $\psi_m(\xi)$ is the mth basis function depicted in Fig. 4, the geometric function becomes finite dimensional

$$\mathbf{F} = (F_1,\ F_2,\ \ldots,\ F_M)^{\mathrm{T}} \tag{25}$$

and the corresponding gradient function ∇J is given by

$$\nabla J = \frac{\partial J}{\partial \mathbf{F}} = \left(\frac{\partial J}{\partial F_1},\ \frac{\partial J}{\partial F_2},\ \ldots,\ \frac{\partial J}{\partial F_M}\right)^{\mathrm{T}} \tag{26}$$

for which the appropriate inner product is

$$\langle \nabla J, \delta \mathbf{F} \rangle = \sum_{m=1}^{M} \left(\frac{\partial J}{\partial F_m}\right)(\delta F_m). \tag{27}$$

The gradient function ∇J can be obtained by introducing the adjoint variables $\mathbf{a}(\xi,\eta,t)$, $r(\xi,\eta,t)$, and $b(\xi,\eta,t)$ such that:

$$\begin{aligned} J = \frac{1}{2}\int_0^{t_f} \sum_{m=1}^{\mathrm{MO}} [T(x_m,y_m) - T^*(x_m,y_m)]^2 \,\mathrm{d}t - \int_0^{t_f}\int_\Omega \mathbf{a}\cdot\left[\sqrt{g}\frac{\partial \mathbf{v}}{\partial t} + \frac{\partial}{\partial \xi^i}(V^i\mathbf{v}) - \frac{\partial}{\partial \xi^i}\left\{ Prg^{ij}\sqrt{g}\frac{\partial \mathbf{v}}{\partial \xi^j}\right\}\right. \\ \left. + \frac{\partial}{\partial \xi^i}(\sqrt{g}\mathbf{g}^i P) - RPr\sqrt{g}T\mathbf{j}\right]\mathrm{d}\Omega\,\mathrm{d}t + \int_0^{t_f}\int_\Omega r\left[\frac{\partial V^i}{\partial \xi^i}\right]\mathrm{d}\Omega\,\mathrm{d}t - \int_0^{t_f}\int_\Omega b\left[\sqrt{g}\frac{\partial T}{\partial t} + \frac{\partial}{\partial \xi^i}(V^i T)\right. \\ \left. - \frac{\partial}{\partial \xi^i}\left\{ g^{ij}\sqrt{g}\frac{\partial T}{\partial \xi^j}\right\}\right]\mathrm{d}\Omega\,\mathrm{d}t, \end{aligned} \tag{28}$$

where the time integration is performed for a sufficiently long period such that steady state is attained at $t = t_f$. Although the identification problems under consideration are steady problems as specified by the objective function, Eq. (21), we introduce time variable in Eq. (28) to derive the unsteady adjoint equations, because it is easier to solve the unsteady adjoint equation to yield the steady-state solution than to solve the steady adjoint equations themselves for the Navier–Stokes problems. Taking the variation of J with respect to F, δJ (cf. Eq. (22)), and integrating δJ by parts and exploiting the boundary conditions, we find that for the steady problems:

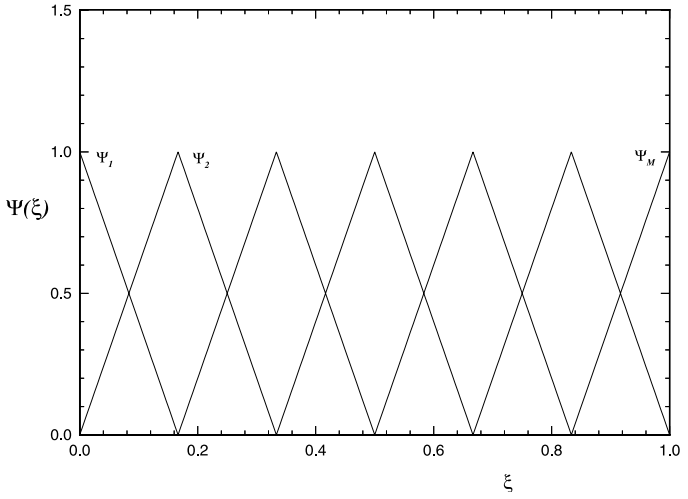

Fig. 4. Basis functions employed to parameterize the unknown boundary shapes.

$$\begin{aligned}\delta J = & \int_\Omega a^y RPrT\delta\sqrt{g}\,\mathrm{d}\Omega + \int_\Omega \left\{ -\left(\frac{\partial \mathbf{a}}{\partial \xi}\right)\cdot\left(\frac{\partial}{\partial \eta}(u\mathbf{v})\right) + \left(\frac{\partial \mathbf{a}}{\partial \eta}\right)\cdot\left(\frac{\partial}{\partial \xi}(u\mathbf{v})\right)\right\}\delta y\,\mathrm{d}\Omega \\ & + \int_\Omega \left\{ -\left(\frac{\partial a^x}{\partial \xi}\frac{\partial p}{\partial \eta} + \frac{\partial a^x}{\partial \eta}\frac{\partial p}{\partial \xi}\right) + \left(-\frac{\partial u}{\partial \xi}\frac{\partial r}{\partial \eta} + \frac{\partial u}{\partial \eta}\frac{\partial r}{\partial \xi}\right)\right\}\delta y\,\mathrm{d}\Omega \\ & + \int_\Omega \left(\frac{\partial (Tu)}{\partial \xi}\frac{\partial b}{\partial \eta} - \frac{\partial (Tu)}{\partial \eta}\frac{\partial b}{\partial \xi}\right)\delta y\,\mathrm{d}\Omega - \int_\Omega \left\{ Pr\left(\frac{\partial \mathbf{a}}{\partial \xi}\right)\cdot\left(\frac{\partial \mathbf{v}}{\partial \xi}\right) + \left(\frac{\partial b}{\partial \xi}\right)\left(\frac{\partial T}{\partial \xi}\right)\right\}\delta(\sqrt{g}g^{11})\,\mathrm{d}\Omega \\ & - \int_\Omega \left\{ Pr\left(\frac{\partial \mathbf{a}}{\partial \xi}\right)\cdot\left(\frac{\partial \mathbf{v}}{\partial \eta}\right) + \left(\frac{\partial b}{\partial \xi}\right)\left(\frac{\partial T}{\partial \eta}\right)\right\}\delta(\sqrt{g}g^{12})\,\mathrm{d}\Omega - \int_\Omega \left\{ Pr\left(\frac{\partial \mathbf{a}}{\partial \eta}\right)\cdot\left(\frac{\partial \mathbf{v}}{\partial \xi}\right)\right. \\ & \left. + \left(\frac{\partial b}{\partial \eta}\right)\left(\frac{\partial T}{\partial \xi}\right)\right\}\delta(\sqrt{g}g^{21})\,\mathrm{d}\Omega - \int_\Omega \left\{ Pr\left(\frac{\partial \mathbf{a}}{\partial \eta}\right)\cdot\left(\frac{\partial \mathbf{v}}{\partial \eta}\right) + \left(\frac{\partial b}{\partial \eta}\right)\left(\frac{\partial T}{\partial \eta}\right)\right\}\delta(\sqrt{g}g^{22})\,\mathrm{d}\Omega, \end{aligned} \tag{29}$$

while the adjoint variables $\mathbf{a}(\xi,\eta,t)$, $r(\xi,\eta,t)$ and $b(\xi,\eta,t)$ must satisfy:

$$\frac{\partial A^i}{\partial \xi^i} = 0, \tag{30}$$

$$\sqrt{g}\frac{\partial \mathbf{a}}{\partial t} + \frac{\partial}{\partial \xi^i}(V^i\mathbf{a}) = -\frac{\partial}{\partial \xi^i}\left[Prg^{ji}\sqrt{g}\frac{\partial \mathbf{a}}{\partial \xi^j}\right] + \frac{\partial}{\partial \xi^i}(\sqrt{g}\mathbf{g}^i r) - T\frac{\partial}{\partial \xi^i}(\sqrt{g}\mathbf{g}^i b) - v_j\frac{\partial}{\partial \xi^i}(\sqrt{g}\mathbf{g}^i a_j), \tag{31}$$

$$\sqrt{g}\frac{\partial b}{\partial t} + \frac{\partial}{\partial \xi^i}(V^i b) = -\frac{\partial}{\partial \xi^i}\left[g^{ji}\sqrt{g}\frac{\partial b}{\partial \xi^j}\right] - a^y RPr\sqrt{g} - \sum_{m=1}^{\mathrm{MO}}[T(x,y) - T^*(x,y)]\delta(x-x_m)\delta(y-y_m), \tag{32}$$

where $\mathbf{a} = a_j = (a^x,\ a^y)^{\mathrm{T}}$

$$\text{and } A^i = \sqrt{g}\mathbf{g}^i\cdot\mathbf{a}. \tag{33}$$

The relevant boundary conditions are:

- $\xi = 0, 1; \quad a^x = a^y = 0, \quad b = 0;$ (34)
- $\eta = 0; \quad a^x = a^y = 0, \quad b = 0;$ (35)
- $\eta = 1; \quad a^x = a^y = 0, \quad \dfrac{\partial b}{\partial \eta} = 0.$ (36)

Once the set of adjoint equations, (30)–(32), is solved, the variation of the objective function δJ is given as a function of the geometric variation terms such as δy, $\delta(\sqrt{g}g^{11})$, etc. The geometric variation terms are obtained by solving the following grid sensitivity equations which are derived from the grid generation equations (15) and (16).

$$\begin{aligned}&(\sqrt{g})^2 g^{11}\frac{\partial^2 \delta x}{\partial \xi^2} + 2(\sqrt{g})^2 g^{12}\frac{\partial^2 \delta x}{\partial \xi \partial \eta} + (\sqrt{g})^2 g^{22}\frac{\partial^2 \delta x}{\partial \eta^2} + \delta\left((\sqrt{g})^2 g^{11}\right)\frac{\partial^2 x}{\partial \xi^2} + 2\delta\left((\sqrt{g})^2 g^{12}\right)\frac{\partial^2 x}{\partial \xi \partial \eta} \\ &\quad + \delta\left((\sqrt{g})^2 g^{22}\right)\frac{\partial^2 x}{\partial \eta^2} = 0, \end{aligned} \tag{37}$$

$$(\sqrt{g})^2 g^{11}\frac{\partial^2 \delta y}{\partial \xi^2} + 2(\sqrt{g})^2 g^{12}\frac{\partial^2 \delta y}{\partial \xi \partial \eta} + (\sqrt{g})^2 g^{22}\frac{\partial^2 \delta y}{\partial \eta^2} + \delta\left((\sqrt{g})^2 g^{11}\right)\frac{\partial^2 y}{\partial \xi^2} + 2\delta\left((\sqrt{g})^2 g^{12}\right)\frac{\partial^2 y}{\partial \xi \partial \eta} + \delta\left((\sqrt{g})^2 g^{22}\right)\frac{\partial^2 y}{\partial \eta^2} = 0, \tag{38}$$

- $\xi = 0, 1; \quad \delta x = 0, \quad \delta y = 0,$ (39)
- $\eta = 0; \quad \delta x = 0, \quad \delta y = \delta F,$ (40)
- $\eta = 1; \quad \delta x = 0, \quad \delta y = 0.$ (41)

In the above equations, the geometric variation terms can be evaluated by exploiting Eqs. (10)–(13). For example,

$$\delta\left((\sqrt{g})^2 g^{11}\right) = 2\left(\frac{\partial x}{\partial \eta}\right)\left(\frac{\partial \delta x}{\partial \eta}\right) + 2\left(\frac{\partial y}{\partial \eta}\right)\left(\frac{\partial \delta y}{\partial \eta}\right). \tag{42}$$

We solve Eqs. (37)–(41) with $\delta F = \psi_1(\xi), \psi_2(\xi), \ldots, \psi_M(\xi)$, where $\psi_i(\xi)$ is the ith basis function depicted in Fig. 4, to obtain $(\delta x_i, \ \delta y_i)^{\mathrm{T}}$, $i = 1, 2, \ldots, M$. In the same way as the geometric function is expressed in terms of the basis functions (cf. Eq. (24)), the geometric variation δF may be written as

$$\delta F = \sum_{m=1}^{M} \delta F_m \psi_m(\xi). \tag{43}$$

Since the grid sensitivity equations, Eqs. (37)–(41), are linear, $(\delta x, \ \delta y)^{\mathrm{T}}$ is obtained easily once $\delta F_m (m = 1, 2, \ldots, M)$ are known.

$$\begin{bmatrix} \delta x \\ \delta y \end{bmatrix} = \sum_{m=1}^{M} \delta F_m \begin{bmatrix} \delta x_m \\ \delta y_m \end{bmatrix}. \tag{44}$$

In this way, all other geometric variation terms are expressed in terms of δF_m. For example,

$$\delta\sqrt{g} = \sum_{m=1}^{M} \delta F_m (\delta\sqrt{g})_m, \tag{45}$$

$$\delta(\sqrt{g} g^{11}) = \sum_{m=1}^{M} \delta F_m \delta(\sqrt{g} g^{11})_m, \tag{46}$$

where

$$(\delta\sqrt{g})_m = \left(\frac{\partial \delta x_m}{\partial \xi}\right)\left(\frac{\partial y}{\partial \eta}\right) + \left(\frac{\partial x}{\partial \xi}\right)\left(\frac{\partial \delta y_m}{\partial \eta}\right) - \left(\frac{\partial \delta x_m}{\partial \eta}\right)\left(\frac{\partial y}{\partial \xi}\right) - \left(\frac{\partial x}{\partial \eta}\right)\left(\frac{\partial \delta y_m}{\partial \xi}\right), \tag{47}$$

$$\delta(\sqrt{g} g^{11})_m = -\frac{(\delta\sqrt{g})_m}{(\sqrt{g})^2}\left\{\left(\frac{\partial x}{\partial \eta}\right)^2 + \left(\frac{\partial y}{\partial \eta}\right)^2\right\} + \frac{1}{\sqrt{g}}\left\{2\left(\frac{\partial x}{\partial \eta}\right)\left(\frac{\partial \delta x_m}{\partial \eta}\right) + 2\left(\frac{\partial y}{\partial \eta}\right)\left(\frac{\partial \delta y_m}{\partial \eta}\right)\right\}. \tag{48}$$

Exploiting Eqs. (45)–(48), the variation of the objective function given in Eq. (29) may be rewritten as

$$\delta J = \sum_{m=1}^{M} \frac{\partial J}{\partial F_m} \delta F_m, \tag{49}$$

where

$$\begin{aligned}
\frac{\partial J}{\partial F_m} \equiv & \int_\Omega a^y RPrT(\delta\sqrt{g})_m \,\mathrm{d}\Omega + \int_\Omega \left\{ -\left(\frac{\partial \mathbf{a}}{\partial \xi}\right) \cdot \left(\frac{\partial}{\partial \eta}(u\mathbf{v})\right) + \left(\frac{\partial \mathbf{a}}{\partial \eta}\right) \cdot \left(\frac{\partial}{\partial \xi}(u\mathbf{v})\right) \right\} \delta y_m \,\mathrm{d}\Omega \\
& + \int_\Omega \left\{ \left(-\frac{\partial a^x}{\partial \xi}\frac{\partial p}{\partial \eta} + \frac{\partial a^x}{\partial \eta}\frac{\partial p}{\partial \xi} \right) + \left(-\frac{\partial u}{\partial \xi}\frac{\partial r}{\partial \eta} + \frac{\partial u}{\partial \eta}\frac{\partial r}{\partial \xi} \right) \right\} \delta y_m \,\mathrm{d}\Omega + \int_\Omega \left(\frac{\partial (Tu)}{\partial \xi}\frac{\partial b}{\partial \eta} \right. \\
& \left. - \frac{\partial (Tu)}{\partial \eta}\frac{\partial b}{\partial \xi} \right) \delta y_m \,\mathrm{d}\Omega - \int_\Omega \left\{ Pr\left(\frac{\partial \mathbf{a}}{\partial \xi}\right) \cdot \left(\frac{\partial \mathbf{v}}{\partial \xi}\right) + \left(\frac{\partial b}{\partial \xi}\right)\left(\frac{\partial T}{\partial \xi}\right) \right\} \delta(\sqrt{g} g^{11})_m \,\mathrm{d}\Omega \\
& - \int_\Omega \left\{ Pr(\frac{\partial \mathbf{a}}{\partial \xi}) \cdot \left(\frac{\partial \mathbf{v}}{\partial \eta}\right) + \left(\frac{\partial b}{\partial \xi}\right)\left(\frac{\partial T}{\partial \eta}\right) \right\} \delta(\sqrt{g} g^{12})_m \,\mathrm{d}\Omega - \int_\Omega \left\{ Pr\left(\frac{\partial \mathbf{a}}{\partial \eta}\right) \cdot \left(\frac{\partial \mathbf{v}}{\partial \xi}\right) \right. \\
& \left. + \left(\frac{\partial b}{\partial \eta}\right)\left(\frac{\partial T}{\partial \xi}\right) \right\} \delta(\sqrt{g} g^{21})_m \,\mathrm{d}\Omega - \int_\Omega \left\{ Pr\left(\frac{\partial \mathbf{a}}{\partial \eta}\right) \cdot \left(\frac{\partial \mathbf{v}}{\partial \eta}\right) + \left(\frac{\partial b}{\partial \eta}\right)\left(\frac{\partial T}{\partial \eta}\right) \right\} \delta(\sqrt{g} g^{22})_m \,\mathrm{d}\Omega.
\end{aligned} \tag{50}$$

In this way the gradient function ∇J is discretized as shown in Eq. (26). The discretization of ∇J converts the infinite dimensional problem into a finite dimensional one, and has an effect of additional regularization as illustrated in [14]. The theoretical basis for the effects of regularization by discretization is well explained in [19].

The basic steps in the application of the Fletcher–Reeves version of the conjugate gradient method applied to the shape identification problems under consideration may be described as follows:

1. Assume $\mathbf{F} = (F_1,\ F_2,\ \ldots,\ F_M)^{\mathrm{T}}$ of $F(\xi)$ and solve the grid generation equation, Eqs. (15) and (16). Then, solve the set of governing equations, Eqs. (7)–(9) until steady state.
2. Solve the set of adjoint equations, Eqs. (30)–(32), until steady state is attained.
3. Solve the grid sensitivity equations, Eqs. (37) and (38), with $\delta F = \psi_1(\xi), \psi_2(\xi), \ldots, \psi_M(\xi)$, respectively, to find $(\delta x_i,\ \delta y_i)^{\mathrm{T}}, i = 1, 2, \ldots, M$. Then, all geometric variational terms can be evaluated as illustrated in Eqs. (45) and (46).
4. The gradient function $\partial J/\partial \mathbf{F}$ is determined by Eq. (50).
5. The conjugate direction vector at the nth iteration stage is given by

$$\mathbf{d}^{(n)} = -\left(\frac{\partial J}{\partial \mathbf{F}}\right)^{(n)} + \varphi^n \mathbf{d}^{(n-1)}, \tag{51}$$

where

$$\varphi^{(0)} = 0, \tag{52}$$

$$\varphi^{(n)} = \frac{\left\langle (\partial J/\partial \mathbf{F})^{(n)}, (\partial J/\partial \mathbf{F})^{(n)} \right\rangle}{\left\langle (\partial J/\partial \mathbf{F})^{(n-1)}, (\partial J/\partial \mathbf{F})^{(n-1)} \right\rangle} \quad (n \geqslant 1). \tag{53}$$

6. Determine the optimal step length ρ^n

$$\rho^n = \arg\min J(\mathbf{F}^{(n)} - \rho^n \mathbf{d}^{(n)}). \tag{54}$$

7. Set

$$\mathbf{F}^{(n+1)} = \mathbf{F}^{(n)} - \rho^n \mathbf{d}^{(n)}. \tag{55}$$

8. If $\langle \mathbf{F}^{(n+1)} - \mathbf{F}^{(n)}, \mathbf{F}^{(n+1)} - \mathbf{F}^{(n)} \rangle$ is less than ϵ, stop. Otherwise, set $n = n + 1$, go to step 2.

The one-dimensional optimization over ρ^n in step 6 is performed by using the golden section search [18] or by employing the following analytic formula

$$\rho^n = \frac{\sum_{m=1}^{\mathrm{MO}} (T(x_m, y_m) - T^*(x_m, y_m))\delta T(x_m, y_m)}{\sum_{m=1}^{\mathrm{MO}} [\delta T(x_m, y_m)]^2}. \tag{56}$$

This is obtained by assuming a quadratic variation of J with respect to ρ^n. The sensitivity field δT is found by solving the sensitivity equations with the relevant boundary conditions.

$$\frac{\partial}{\partial \xi^i}(\delta V^i) = 0, \tag{57}$$

$$\sqrt{g}\frac{\partial}{\partial t}\delta \mathbf{v} + \frac{\partial}{\partial \xi^i}(V^i \delta \mathbf{v}) = \frac{\partial}{\partial \xi^i}\left\{ Pr g^{ij}\sqrt{g}\frac{\partial \delta \mathbf{v}}{\partial \xi^j} \right\} + \mathbf{S}^p + \sqrt{g} RPr \delta T \mathbf{j} + \mathbf{S}^{\mathbf{v}}, \tag{58}$$

$$\sqrt{g}\frac{\partial}{\partial t}\delta T + \frac{\partial}{\partial \xi^i}(V^i \delta T) = \frac{\partial}{\partial \xi^i}\left\{ g^{ij}\sqrt{g}\frac{\partial \delta T}{\partial \xi^j} \right\} + S^{\mathrm{T}}, \tag{59}$$

where $\delta \mathbf{v}$ and δT are the deviational velocity and deviational temperature field, respectively, which indicate the sensitivity of the velocity and temperature fields with respect to the variation of the geometry δF. The deviational contravariant velocity is defined by:

$$\delta V^i = \sqrt{g}\mathbf{g}^i \cdot \delta \mathbf{v} + \delta.(\sqrt{g}\mathbf{g}^i) \cdot \mathbf{v} \tag{60}$$

Source terms S^p, $\mathbf{S}^{\mathbf{v}}$ and S^{T} in Eqs. (58) and (59) are given by:

$$\mathbf{S}^p = -\frac{\partial}{\partial \xi^i}(\sqrt{g}\mathbf{g}^i \delta P) - \frac{\partial}{\partial \xi^i}(\delta(\sqrt{g}\mathbf{g}^i)P), \tag{61}$$

$$\mathbf{S}^{\mathbf{v}} = -\frac{\partial}{\partial \xi^i}(\delta V^i \mathbf{v}) + \frac{\partial}{\partial \xi^i}\left[Pr\delta(g^{ij}\sqrt{g})\frac{\partial \mathbf{v}}{\partial \xi^j} \right] + \frac{\delta\sqrt{g}}{\sqrt{g}}\left[\frac{\partial}{\partial \xi^i}(V^i \mathbf{v}) - \frac{\partial}{\partial \xi^i}\left\{ Pr g^{ij}\sqrt{g}\frac{\partial \mathbf{v}}{\partial \xi^j} \right\} \right], \tag{62}$$

$$S^{\mathrm{T}} = -\frac{\partial}{\partial \xi^i}(\delta V^i T) + \frac{\partial}{\partial \xi^i}\left[\delta(g^{ij}\sqrt{g})\frac{\partial T}{\partial \xi^j} \right] + \frac{\delta\sqrt{g}}{\sqrt{g}}\left[\frac{\partial}{\partial \xi^i}(V^i T) - \frac{\partial}{\partial \xi^i}\left\{ g^{ij}\sqrt{g}\frac{\partial T}{\partial \xi^j} \right\} \right], \tag{63}$$

where

$$\delta\sqrt{g} = \frac{\partial \delta x}{\partial \xi}\frac{\partial y}{\partial \eta} + \frac{\partial x}{\partial \xi}\frac{\partial \delta y}{\partial \eta} - \frac{\partial \delta y}{\partial \xi}\frac{\partial x}{\partial \eta} - \frac{\partial y}{\partial \xi}\frac{\partial \delta x}{\partial \eta} \tag{64}$$

and henceforth. The boundary conditions for the sensitivity equations are

- on $\partial\Omega_1$; $\quad \delta \mathbf{v} = 0, \quad \delta T = 0,$ (65)
- on $\partial\Omega_2$; $\quad \delta \mathbf{v} = 0, \quad \delta T = 0,$ (66)
- on $\partial\Omega_3$; $\quad \delta \mathbf{v} = 0, \quad \left(\frac{\partial \delta T}{\partial y}\right) = 0,$ (67)

• on $\partial\Omega_4$; $\delta\mathbf{v} = 0$, $\delta T = 0$. (68)

We employ (40×20) grids for the finite volume method to solve the governing equations, adjoint equations and sensitivity equations, which is found to be sufficient to resolve the fields.

4. Results

In the present investigation, we employ the simulated experimental data. Namely, we solve the governing equations, Eqs. (7)–(9), numerically, and adopt the numerical solution at the measurement locations as experimental data after adding a certain amount of random errors. As a first attempt to test the present algorithm, we consider the idealized situations where there are no measurement error. The three geometries depicted in Figs. 2(a)–(c) are investigated, where $R = 2000.0$ and $Pr = 0.72$. Since the dimensionless height of the domains is 1.5, the actual Rayleigh number is 6750. The bottom boundary $\partial\Omega_1$ is parameterized with seven basis functions (cf. Eq. (24)) and temperature is measured at nine equidistant locations on the top boundary $\partial\Omega_3$ as depicted in Fig. 2. The initially assumed shapes in the conjugate gradient iterations are the rectangles as shown in Fig. 2 with dashed lines. The estimation error is defined by

$$\text{Estimation error} = \frac{\|F(\xi)^{\text{exact}} - F(\xi)^{\text{estimated}}\|_2}{\|F(\xi)^{\text{exact}}\|_2}, \tag{69}$$

where $\|\cdot\|_2$ is the usual L_2-norm. Figs. 5(a) and (b) show the convergence rate of the conjugate gradient method for the case of Fig. 2(a) where the detailed shapes of the identified domain (Fig. 5(a)) with the corresponding estimation errors (Fig. 5(b)) are depicted. It is shown that almost exact shape is identified in 21 iterations with the estimation error of 0.0658. Figs. 6(a) and (b) show the identified shapes for the case of Figs. 2(b) and (c) The estimation errors and corresponding iteration numbers required before convergence are also shown in the same figures.

The effect of number of measurement locations on the accuracy of estimation is investigated. Fig. 7 shows the identified shape for the case of Fig. 2(a) when the number of equidistant measurement locations on $\partial\Omega_3$ is increased from the default value of 9–18. Comparing this result with the reference one, Fig. 5, obtained with nine equidistant measurement locations, it is found that the accuracy of estimation improves as the number of measurement locations increases. Final consideration is the effect of measurement error on the accuracy of estimation. Since measurement error is inevitable in all practical situations, it is important to confirm that the present method still identifies the shape reasonably accurately even if the temperature measurements are corrupted by noise. Corrupted measurements are generated by adding Gaussian distributed random noise to the simulated measurements that are the exact numerical solution at the measurement locations. When there are measurement errors, the following discrepancy principle is adopted as the stopping criterion of the conjugate gradient iteration [20]. Assuming the measurement errors to be the same for all measurements, Eq. (21) becomes

$$J \approx \frac{1}{2}\sum_{m=1}^{\text{MO}} \sigma^2 = \epsilon^2, \tag{70}$$

where σ is the magnitude of measurement error at each measurement location. Then the discrepancy principle for the stopping criterion is taken as

$$J \leqslant \epsilon^2. \tag{71}$$

If the function J has a minimum value that is larger than ϵ^2 the following criterion is used to stop the iteration.

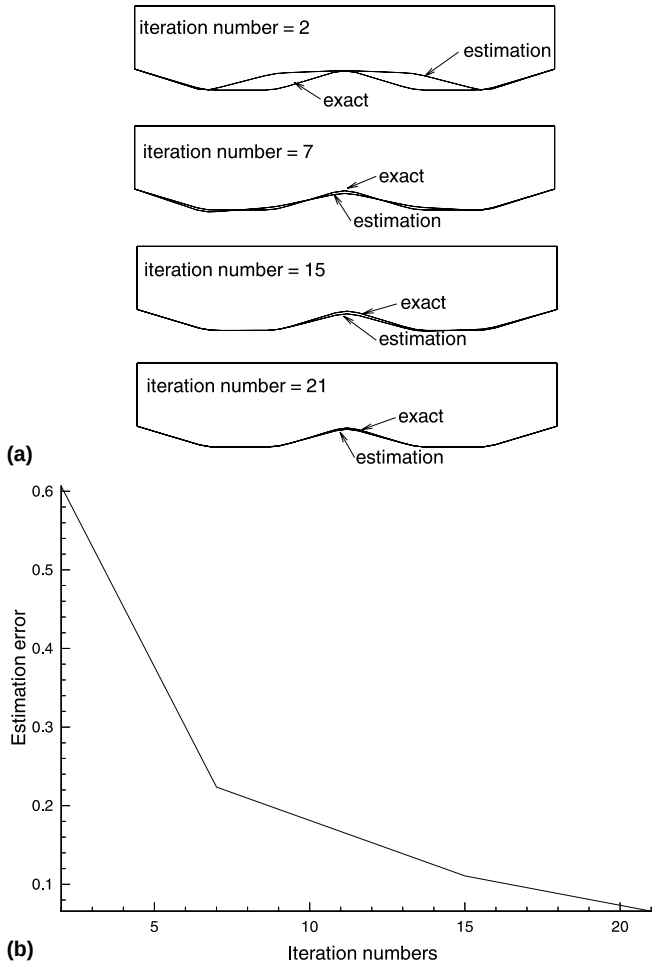

Fig. 5. Variation of the shape (a) and estimation error (b) for the case of Fig. 2(a).

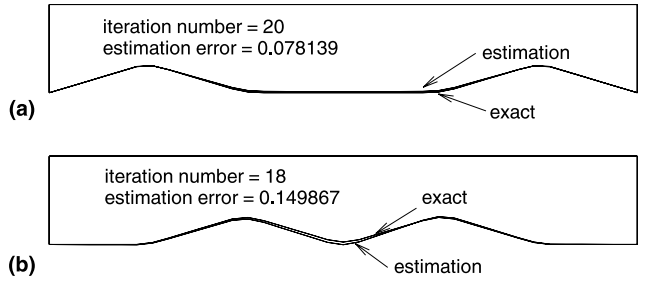

Fig. 6. Identified shapes for the cases of Figs. 2(b) and (c). The case of (a) Fig. 2(b) and (b) Fig. 2(c).

$$J(\mathbf{F}^{(i+1)}) - J(\mathbf{F}^{(i)}) \leqslant \epsilon_1, \tag{72}$$

where ϵ_1 is a prescribed small number. Figs. 8(a) and (b) show the estimated shapes for the case of Fig. 2(a) when the relative measurement error is 0.1% (Fig. 8(a)) and 0.3% (Fig. 8(b)), respectively. Comparing these

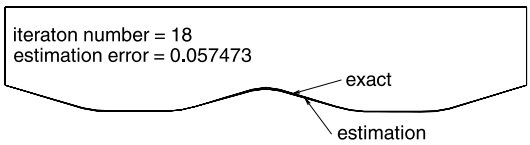

Fig. 7. Identified shape for the case of Fig. 2(a) when the number of measurement locations is increased to 18.

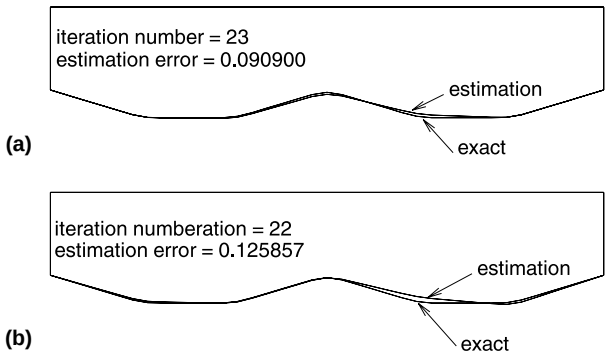

Fig. 8. Effect of measurement error on the accuracy of estimation. 0.1% (a) and 0.3% (b) relative measurement error.

results with that of Fig. 5, where the measurements are exact, we get the expected conclusion that the accuracy of estimation deteriorates as the measurement error increases.

5. Conclusion

A method of identifying the boundary shape of a domain, where the temperature field is dominated by natural convection, from temperature measurements on the other boundary is investigated. After mapping the irregular domains into a reference one using a set of parameters, the inverse problem is formulated as a parameter optimization problem of the output least-squares criterion, which is solved by a conjugate gradient method employing the adjoint variable method. The potential applications of the present investigation are the thermal tomography, which detects structural flaws caused by corrosion nondestructively, and the identification of a phase change isotherm in Bridgman growth of semiconductor materials. The effects of number of measurement locations and measurement errors on the accuracy of estimation are also investigated. The present method is found to identify the domains reasonably accurately even with noisy temperature measurements.

Acknowledgement

This work was supported by the Korea Research Foundation (KRF-2002-005-D00010).

References

[1] J.V. Beck, B. Blackwell, C.St. Clair, Inverse Heat Conduction: Ill-posed Problems, Wiley-Interscience, New York, 1985.
[2] D.M. Heath, C.S. Welch, W.P. Winfree, Quantitative thermal diffusivity measurements of composites, in: Rev. Prog. Quant. Nondestructive Eval., vol. 5B, Plenum Publ., New York, 1986, pp. 1125–1132.

[3] S.A. Campbell, The Science and Engineering of Microelectronic Fabrication, Oxford University Press, Oxford, 1996.
[4] M. Flemings, Solidification Processing, McGraw-ill, New York, 1974.
[5] O. Pironneau, Optimal Shape Design for Elliptic Systems, Springer-Verlag, New York, 1983.
[6] S. Chen, D.A. Tortorelli, Three-dimensional shape optimization with variational geometry, Struct. Opt. 13 (1997) 81.
[7] K.-H. Chang, K.K. Choi, C.-S. Tsai, C.-J. Chen, B.S. Choi, X. Yu, Design sensitivity analysis and optimization tool (DSO) for shape design applications, Comput. Syst. Eng. 6 (1995) 151.
[8] Z.-X. Wang, D.A. Tortorelli, J.A. Danzig, Sensitivity analysis and optimization of coupled thermal and flow problems with applications to contraction design, Int. J. Numer. Methods Fluids 23 (1996) 991.
[9] C.-H. Huang, B.-H. Chao, An inverse geometry problem in identifying irregular boundary configurations, Int. J. Heat Mass Transfer 40 (1997) 2045.
[10] G.S. Dulikravich, T.J. Martin, Inverse design of super-elliptic cooling passages in coated turbine blade airfoil, J. Thermophys. Heat Transfer 8 (1994) 288.
[11] E. Beretta, S. Vessella, Stable determination of boundaries from Cauchy data, SIAM J. Math. Anal. 30 (1990) 220.
[12] M. Burger, H.W. Engl, P. Markowich, P. Petra, Identification of doping profiles in semiconductor devices, Inverse Problems 17 (2001) 765.
[13] G. Yang, N.A. Zabaras, A functional optimization formulation and implementation of an inverse natural convection problem, Comput. Methods Appl. Mech. Eng. 144 (1997) 245.
[14] H.M. Park, O.Y. Chung, On the solution of an inverse natural convection problem using various conjugate gradient methods, Int. J. Numer. Methods Eng. 47 (2000) 821.
[15] S.V. Patankar, Numerical Heat Transfer and Fluid Flow, McGraw-Hill, New York, 1980.
[16] C.M. Rhie, W.L. Chow, A numerical study of the turbulent flow past an isolated airfoil with trailing edge separation, AIAA J. 21 (1983) 1525.
[17] J.F. Thompson, Z.U.A. Warsi, Numerical Grid Generation, North-Holland, The Netherlands, 1985.
[18] D.G. Luenberger, Linear and Nonlinear Programming, second ed., Addison-Wesley, Reading, MA, 1984.
[19] H.W. Engl, M. Hanke, A. Neubauer, Regularization of Inverse Problems, Kluwer Academic Publisher, Dordrecht, 1996.
[20] O.M. Alifanov, Application of the regularization principle to the formulation of approximate solution of inverse heat conduction problem, J. Eng. Phys. 23 (1972) 1566.